

Beyond Memorization: A Multi-Modal Ordinal Regression Benchmark to Expose Popularity Bias in Vision-Language Models

Li-Zhong Szu-Tu[†] Ting-Lin Wu[†] Chia-Jui Chang He Syu Yu-Lun Liu

National Yang Ming Chiao Tung University

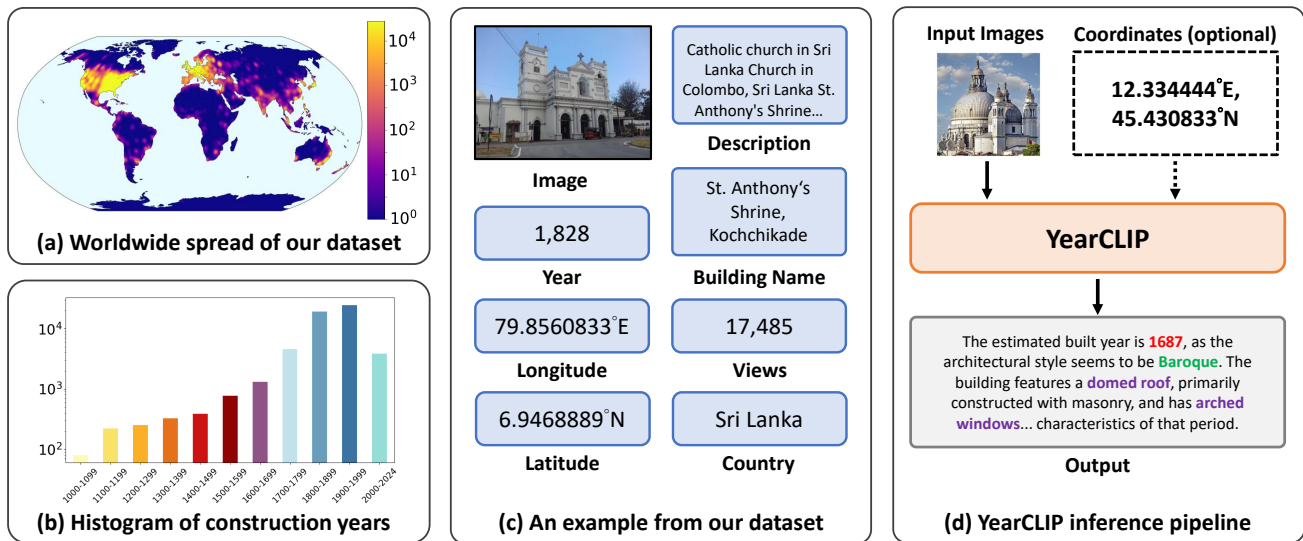


Figure 1. Overview of **YEARGUESSR** and **YearCLIP**. (a) Global distribution of the 55k Wikipedia-sourced building images. (b) Log-scale histogram of construction years spanning 1001–2024 CE. (c) Display all the attributes with an example in **YEARGUESSR** (d) Given an image and optional GPS coordinates, **YearCLIP** returns the estimated construction year together with an architectural rationale.

Abstract

We expose a significant popularity bias in state-of-the-art vision-language models (VLMs), which achieve up to 34% higher accuracy on famous buildings compared to ordinary ones, indicating a reliance on memorization over generalizable understanding. To systematically investigate this, we introduce the largest open benchmark for this task: the **YearGuessr** dataset, a collection of 55,546 building images with multi-modal attributes from 157 countries, annotated with continuous ordinal labels of their construction year (1001–2024), GPS data, and page-view counts as a proxy for popularity. Using this dataset, we frame the construction year prediction task as ordinal regression and introduce popularity-aware interval accuracy metrics to quantify this bias. Our resulting benchmark of 30+ models, including our **YearCLIP** model, confirms that VLMs excel on popular,

memorized items but struggle significantly with unrecognized subjects, exposing a critical flaw in their reasoning capabilities. Project page: <https://sytwu.github.io/BeyondMemo/>

1. Introduction

The construction year of a building is essential for sustainability audits, heritage preservation, and post-disaster assessment. Yet, unlike style or material, the age of most of the world’s 1.5 trillion mapped buildings is unknown. Automated *building age estimation* could support continent-scale retrofitting and fine-grained historical queries, but progress is hindered by the lack of a global, large-scale, open benchmark. Figure 1 previews **YearGuessr**, our answer to this gap.

As shown in Table 1, existing datasets are either geographically narrow or temporally shallow. **MyCD** dataset [14] covers only Western Europe with coarse epochs (<1930,

[†]Equal contribution.

Table 1. **Building-age datasets.** Earlier datasets are either regional, post-1900, have no images, or are closed source. Our YEARGUESSR will be the first CC BY-SA 4.0 image set with continuous labels, global (157 countries) coverage, and a 1001~2024 CE span.

Dataset	Region(s)	Year span	Size	Modalities	Continuous labels	Images	Open?
MyCD [14]	Europe	<1930 ~ >2006	32k img	SVI, VHR, MSI		✓	✓
CMAB [79]	China	1985 ~ 2018	29M bldg	RS, SVI, GIS, HS	✓		✓
MTBF-33 [60]	USA (33 counties)	1900 ~ 2015	6.2M img	Footprints (SHP)	✓	✓	✓
ResBldgAge [49]	UK	<1915 ~ >1980	2.5k img	Maps, census		✓	
3D-GIS Age [8]	NL	1860 ~ 2017	35k bldg	LOD1 3-D GIS	✓		
UrbanFormAge [45]	NL, FR, ES	<1945 ~ 2010	25.3M img	OSM, 2-D urban form	✓	✓	✓
GPT-4V London [74]	London	<1700 ~ >2020	131 img	Facade + attrs		✓	✓
PhotoAge [75]	Austria	1960s ~ 2010s	11.1k img	real estate, web	✓	✓	
StreetViewAge [57]	NL (AMS)	1300 ~ 2000	39k img	SVI + BAG		✓	✓
WikiChurches [5]	Europe	401 ~ 2011	9.5k img	Wikipedia facades	✓	✓	✓
YEARGUESSR (ours)	157 countries	1001 ~ 2024	55.5k img	Wikipedia facades	✓	✓	✓

1930~1959, ...), CMAB [79] is restricted to modern Chinese facades and narrow temporal range (1985~2018), MTBF-33 [74] lacks photographs, and others remain geographically or temporally narrow. Prior works also cast age prediction as classification, ignoring temporal ordinality, while licensing restrictions impede reproducibility.

Beyond data gaps, a fundamental question remains: *do vision-language models (VLMs) truly learn architecture, or simply memorize landmarks?* We show that VLMs like Gemini-2.0 gain +34.18% accuracy on high-popularity buildings, whereas other general models degrade (Section 5). It depicts the evidence of *popularity memorization* rather than genuine architectural understanding.

To address these issues, we present YearGuessr, the first open benchmark for building-age estimation with 55,546 images across 157 countries, spanning 1001–2024 CE in Figure 1(a) and (b), along with our proposed model, YearCLIP. Each entry includes facades, GPS, captions, and Wikipedia page views to probe memorization bias. We frame the task as ordinal regression and evaluate with MAE, Interval Accuracy, and a new popularity-aware metric, demonstrating that VLMs’ performance might stem from memorization rather than architectural understanding potentially.

Our YearCLIP (Section 4) is a CLIP-based model that integrates ordinal training using a coarse-to-fine strategy from NumCLIP [16], and GPS priors via a fused location encoder with zero-convolution. It is also notably enhanced with several pre-defined reasoning prompts (e.g., Roof (spire, dome), Wall (brick, stone)) that enrich the feature space. This allows the model to provide human-verifiable rationales by highlighting the most relevant architectural cues, adding a crucial layer of explainability to its final year prediction.

Our contributions are:

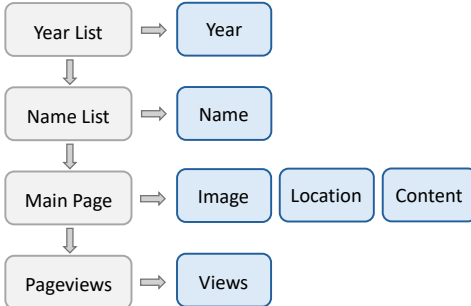
- **YearGuessr dataset:** will be the first open, CC BY-SA 4.0 corpus with global coverage, large-scale ordinal labels, GPS, and rich textual descriptions.
- **YearCLIP model:** We propose YearCLIP, our baseline model, which is enhanced with reasoning prompts to provide explainability for the age prediction task.

- **Evaluation protocol:** an original regression benchmark with Interval Accuracy and a new popularity-based MAE metric to quantify memorization bias.
- **Baseline:** We provide a comprehensive benchmark study of 30+ CNN-, Transformer-, CLIP-based, and LLM/VLM models.
- **Insights:** We reveal that VLMs memorize popular landmarks, achieving dramatically different performance based on building fame rather than architectural features.

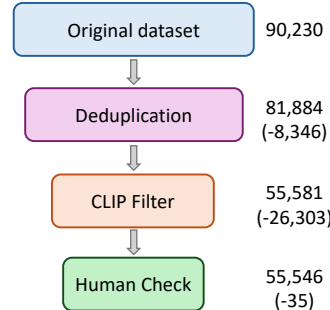
2. Related Work

Datasets for building-age estimation. Prior corpora remain limited in scope. Building Age Estimation [14] fuses multiple modalities but covers only Western Europe and coarse epochs. CMAB adds Chinese façades yet spans 1985–2018 [79]. MTBF-33 lists U.S. footprints without imagery [60]. Other efforts are small-scale (131 London photos [74]) or style-focused (WikiChurches [5]). Early work on architectural style recognition [40–42] and heritage analysis [38] established foundations for visual classification. Broader surveys [17] situate AI in preservation. Earlier datasets often rely on real-estate photos or GIS metadata [8, 32, 57]. In contrast, YEARGUESSR contributes 55k Wikipedia-sourced CC-BY-SA images spanning 1001–2024 CE across six continents, following best practices from WIT [56].

Image geolocalization foundations. Planet-scale localization began with Im2GPS [23] and PlaNet [68], later refined via hierarchical cells [52, 62], scene cues [44], and segmentation [47, 69]. Recent work integrates transformers [12], cross-view supervision [6, 28, 82], and human traces [39]. Related building-attribute studies predict materials, structure, or energy efficiency [7, 13, 53]. Advanced façade parsing [34, 76] highlights age-indicative elements. Despite progress, these pipelines stop short of fine-grained building-age dating.



(a) Data Collection Pipeline



(b) Data Cleaning Pipeline



(c) Data Cleaning Example

Figure 2. **Data collection and cleaning pipeline.** (a) We crawl the Wikipedia category tree of buildings, collecting façade images, construction years, GPS coordinates, textual descriptions, and pageview statistics. (b) The raw crawl of 90k images is refined through deduplication, a CLIP-based building filter, and a light manual audit, yielding 55k clean façades. (c) Examples of discarded non-building or duplicate samples.

Geo-aware VLMs. Contrastive VLMs lack strong spatial priors. GeoCLIP [61], LLMGeo [67], GeoReasoner [29], PIGEON [22], and SPF [27] incorporate coordinates or climate. SNAP [51] uses map tiles, while AddressCLIP [71] aligns directly with street addresses. Metadata-image fusion shows promise (e.g., EXIF-as-language [81]), paralleling our approach. Yet our evaluation also reveals popularity bias [80], echoing dataset bias studies [54, 63].

Ordinal regression with numeric cues. Ordinal regression evolved from CORAL/CORN losses [9, 46] to order-regularised and probabilistic methods [21, 30, 55]. Classification with discretization [18] proved effective for continuous estimation. Vision-language extensions (OrdinalCLIP [31], NumCLIP [16]) encode order in text. Related applications include age [50], depth [64, 78], and counts [33]. We extend this line by evaluating CLIP and GPT-4V [2] on large-scale building ages.

Multi-modal learning signals. Auxiliary cues such as weather, land cover, or captions [22, 48, 72] aid localization. WikiTiLo [77] shows VLMs still lack temporal–geo knowledge, motivating visual chain-of-thought prompting [11] or open-vocabulary 3D understanding [26]. Bias mitigation strategies [66] and diversity concerns [54] remain critical. Inspired by NeRF’s RFFs [43], we combine coordinate encodings with ordinal losses to achieve state-of-the-art on YearGuesser.

3. Dataset and Benchmark

3.1. Dataset Construction

Data sources and licences. All images and textual descriptions are scraped from *Wikipedia* and its sister project *Wikimedia Commons*. Both platforms distribute user-contributed content primarily under the CC BY-SA 4.0 or Public-Domain

licences, which permit redistribution provided attribution is preserved. During crawling, we query the Commons API for the exact licence of every file and discard items tagged as “*non-free*” or “*no derivatives*”. Consequently, the **YearGuesser** corpus (images, metadata, and split indices) will be publicly available under the same CC BY-SA 4.0. The accompanying code will be publicly available under the MIT license.

Automatic collection pipeline. Figure 2 (a) illustrates the four-stage crawler. (1) We begin by recursively traversing the `Buildings_and_structures_by_year_of_completion` category on Wikimedia Commons, dated from 1001 CE to 2024. (2) It collects 90,230 pages related to buildings and structures from the category. (3) For every building page, we extract the first infobox image, geographic coordinates, and full wikitext. (4) We call the Wikimedia Pageviews API to obtain the total number of views between 01 Jul 2023 and 01 Jul 2024, which we later use as a proxy for *popularity*.

Cleaning and quality control. We remove duplicates, off-topic images, and irrelevant files via the Figure 2 pipeline. First, deduplication retains one image per page title, eliminating 8,346 duplicates. Next, a ViT-B/32 CLIP filter scores similarity to “a building facade” and drops 26,338 low matches. Finally, a brief manual audit of the test split removes 35 obvious outliers (e.g., aircraft, interiors). This leaves 55,546 unique, high-quality facade images, each representing a distinct building.

Train/validation/test split. We stratify by *construction decade* and *continent* and then assign 60% / 20% / 20% of buildings to the training, validation and test partitions, respectively, resulting in 33,337 / 11,122 / 11,087 samples. No building, caption, or image appears in more than one

<https://en.wikipedia.org/wiki/Wikipedia:Copyrights>

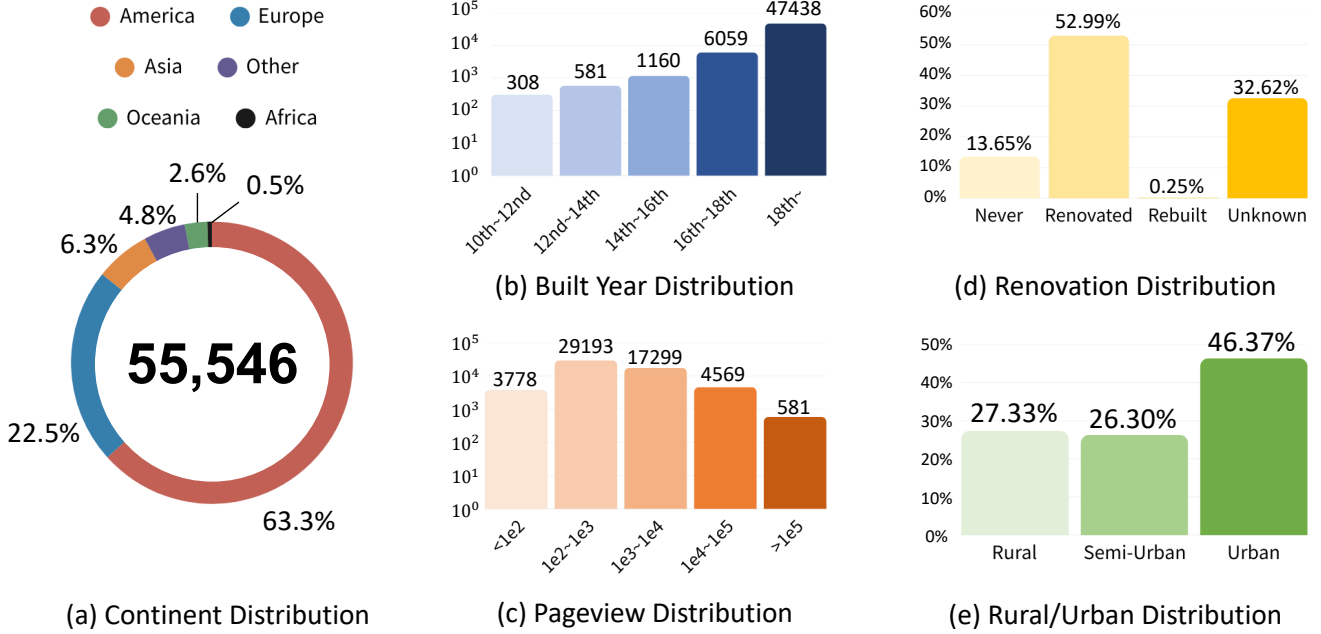


Figure 3. **Dataset statistics.** This figure provides an overview of our dataset’s key characteristics. (a) Continent Distribution shows the geographical origins of the images. (b) Built Year Distribution illustrates the age of the structures. (c) Pageview Distribution represents the buildings’ popularity. (d) Renovation Distribution indicates the extent of reconstruction. (e) Rural/Urban Distribution reflects the population density of a building’s location.

split.

Metadata completeness. All samples include GPS coordinates (100%), country name (via reverse-geocoding), and textual description (median length 2,240 characters). Figure 1 (b) shows the year distribution spanning 1,000 years. Figure 1 (a) shows geographical spread across 157 countries.

3.2. Statistics Analysis

Geographic Distribution. Our dataset spans 157 nations, but it is heavily skewed toward the Americas (63.3%) and Europe (22.5%). Asia accounts for 6.3%, while Oceania and Africa make up a smaller fraction. This geographical imbalance, visualized in Figure 3(a), motivates us to report continent-specific evaluation metrics in later sections.

Temporal Distribution. Figure 3(b) illustrates the age of the structures in our dataset. There’s a notable concentration of buildings constructed in the 18th century and later. The dataset also includes a significant number of pre-1600 buildings, which enables large-scale historical analysis.

Building Popularity. We use a building’s Wikipedia pageviews as a proxy for its popularity. Figure 3(c) shows a heavy-tailed distribution: a large number of images have low annual views, while a small subset of highly viewed landmarks (e.g., over 10,000 views) represent a significant portion of the corpus. This skew is a key characteristic of our dataset.

Renovation Scenario. Figure 3(d) summarizes building reconstruction status. Most (52.99%) show no renovation, while 32.62% lack historical records. We distinguish between *renovated* buildings, where the original construction year remains valid, and *rebuilt* buildings, where the construction year is effectively redefined. Annotations were extracted via LLM analysis of building descriptions.

Rural/Urban Regions. Figure 3(e) reports location categories derived by mapping coordinates to GPWv4.11 population density. Buildings are classified as *Rural* (<300 people/km 2), *Semi-urban* (300–1500 people/km 2), or *Urban* (>1500 people/km 2), providing finer-grained geographical context.

3.3. Tasks & Metrics

Problem Formulation. Given a facade image I and optional GPS coordinates $g = (\phi, \lambda)$, the primary task is to predict *construction year* $y \in \mathbb{Z}$ of the building depicted. Following Niu et al. [46] and Cao et al. [9], we cast the problem as **ordinal regression** rather than hard classification or naïve regression. Formally, a model f_θ outputs a scalar $\hat{y} = f_\theta(I, g)$ and may additionally emit a text rationale \hat{r} (Section 5).

Evaluation Metrics and Protocol.

Mean Absolute Error: $MAE = \frac{1}{N} \sum_{i=1}^N |y_i - \hat{y}_i|$.

Interval Accuracy: $IA_k = \frac{1}{N} \sum_{i=1}^N \mathbb{1}[|y_i - \hat{y}_i| \leq k]$ for $k \in$

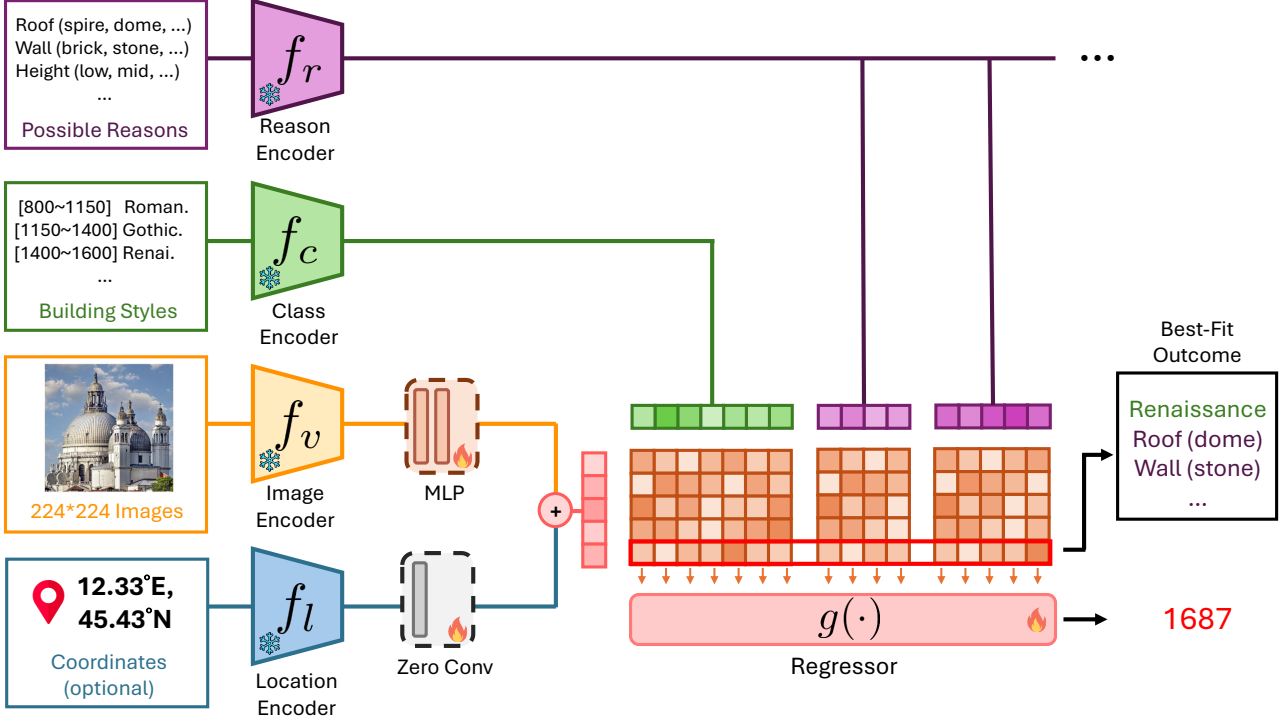


Figure 4. **YEARCLIP architecture.** An image encoder f_v (CLIP) extracts 224×224 facade features. We then fuse the feature with a GPS embedding from the location encoder f_l (RFF + MLP, optional input) via a learnable zero-convolution. Parallel text branches encode (i) seven coarse style classes f_c and (ii) a bank of reasoning prompts f_r describing roofs, walls, heights, etc. All frozen encoders feed a trainable regressor $g(\cdot)$ that performs coarse-to-fine ordinal regression. It predicts a construction year (here 1687), selects the best-matching style/reason tokens, and outputs a readable rationale.

$\{5, 20, 50, 100\}$ years. IA₂₀ approximates ‘‘gets the right architectural period’’; IA₅ rewards near exact dating. All metrics are computed in the fixed test split (11,087 images as mentioned in Section 3.1). For models that consume GPS, both *with-* and *without-*location scores are reported to expose the benefit and potential leakage of spatial priors. We repeat every experiment with three random seeds and report the mean and standard deviation.

4. Our YearCLIP Model

Model architecture. Traditional models for image-based tasks often rely on CNNs or Transformers. Instead, we use CLIP [48], a multi-modal framework pre-trained to align image and text, ideal for the semantically rich task of building age prediction due to its zero-shot generalization to under-represented periods. To combine CLIP with ordinal regression, we adopt NumCLIP [16], which uses language priors for a coarse-to-fine strategy. It first classifies architectural styles coarsely, then computes similarity scores for a regressor to predict fine-grained years, balancing style recognition with temporal precision. The overall pipeline design is shown as Figure 4.

Location conditioning. The GeoReasoner framework [29] indicates that building images degrade performance in geographic location prediction, likely due to colonial influences or style imitation across regions. Geographic context, however, provides cues absent in visual data, enhancing architectural style interpretation for age estimation. We utilize the pretrained location encoder from GeoCLIP [61] and fuse location and image embeddings in the latent space to integrate spatial information. For images lacking location data, which is a common scenario, we rely solely on image embeddings for similarity computation, ensuring model flexibility.

Zero convolution. Fusing image and location embeddings via a weighting parameter α is straightforward but challenging to optimize manually. Instead, we add a zero convolution layer post-location encoder, enabling the model to learn optimal weights autonomously during training, improving fusion effectiveness.

Reasoning prompt integration. Unlike the original NumCLIP, which relies solely on category similarity for regression, we augment the regressor with pre-defined reasoning prompts. These prompts, encoded via a text encoder, enrich the input feature space, enabling more accurate year predictions. Additionally, the regressor can backtrack the

Table 2. Performance on basic metric, interval accuracy, and popularity analysis (simplified). Please refer to supplementary material for a complete evaluation of all 43 methods.

Method	Model	Basic		Interval Accuracy		Popularity (IA_5)		
		MAE (↓)		≤ 5 (↑)	≤ 100 (↑)	$< 10^2$ (↑)	$> 10^5$ (↑)	Gain
CNN	ResNet-50 [24]	54.14 ± 0.47		10.44 ± 0.56	88.68 ± 0.41	12.39 ± 1.38	9.14 ± 0.51	-3.25 ± 1.60
	ConvNeXt-B [37]	44.42 ± 0.33		14.01 ± 0.56	90.72 ± 0.07	16.57 ± 0.94	12.68 ± 3.11	-3.89 ± 3.58
Transformer	ViT-B/16 [15]	49.16 ± 0.43		12.50 ± 0.51	89.52 ± 0.42	15.82 ± 0.85	6.78 ± 1.84	-9.04 ± 1.75
	Swin-B [36]	47.65 ± 0.67		12.65 ± 0.68	89.95 ± 0.19	15.92 ± 2.27	9.14 ± 0.51	-6.77 ± 1.88
CLIP-based	CLIP (zero-shot) [48]	78.23 ± 0.00		12.78 ± 0.00	78.55 ± 0.00	13.52 ± 0.00	7.96 ± 0.00	-5.56 ± 0.00
	GeoCLIP [61]	45.69 ± 0.49		23.79 ± 0.26	89.54 ± 0.11	24.37 ± 1.06	19.17 ± 1.35	-5.19 ± 0.91
	NumCLIP [16]	40.01 ± 0.55		18.15 ± 0.31	91.76 ± 0.16	21.69 ± 1.62	11.80 ± 3.58	-9.89 ± 2.42
	YearCLIP (ours)	39.52 ± 0.27		18.93 ± 0.75	91.63 ± 0.44	20.19 ± 0.94	12.39 ± 3.86	-7.80 ± 4.26
Closed VLMs	GPT4o-mini [2]	42.69 ± 0.00		22.75 ± 0.00	89.62 ± 0.00	19.01 ± 0.00	48.67 ± 0.00	29.66 ± 0.00
	Gemini1.5-pro [19]	33.08 ± 0.00		28.18 ± 0.00	93.14 ± 0.00	26.76 ± 0.00	43.36 ± 0.00	16.60 ± 0.00
	Gemini2.0-flash [20]	33.91 ± 0.00		29.71 ± 0.00	92.75 ± 0.00	24.23 ± 0.00	58.41 ± 0.00	34.18 ± 0.00
	Claude3-haiku [3]	47.88 ± 0.00		16.13 ± 0.00	88.47 ± 0.00	18.45 ± 0.00	32.74 ± 0.00	14.29 ± 0.00
	Grok2 [70]	35.28 ± 0.00		27.57 ± 0.00	93.02 ± 0.00	25.77 ± 0.00	42.48 ± 0.00	16.71 ± 0.00
OpenVLM	CogVLM2-19B [25]	42.50 ± 0.52		18.63 ± 0.30	90.57 ± 0.18	18.31 ± 1.25	23.01 ± 1.77	4.70 ± 2.99
	Gemma3-27B [58]	36.48 ± 0.00		25.58 ± 0.00	92.53 ± 0.00	24.37 ± 0.00	41.59 ± 0.00	17.22 ± 0.00
	GLM-4v-9B [65]	38.13 ± 0.06		19.96 ± 0.05	91.81 ± 0.08	18.50 ± 0.35	25.37 ± 0.51	6.87 ± 0.84
	InternVL2-26B [10]	129.39 ± 7.84		16.75 ± 0.15	85.83 ± 0.18	14.13 ± 1.13	26.25 ± 3.58	12.12 ± 4.70
	InternVL3-38B [10]	63.18 ± 2.45		20.29 ± 0.26	90.32 ± 0.18	17.09 ± 1.07	28.32 ± 0.89	11.23 ± 1.47
	LLaVA15-13B [35]	60.26 ± 0.00		10.74 ± 0.00	84.21 ± 0.00	7.75 ± 0.00	16.81 ± 0.00	9.06 ± 0.00
	LLaVA-v16-13B [35]	194.07 ± 0.00		12.13 ± 0.00	80.38 ± 0.00	12.82 ± 0.00	15.04 ± 0.00	3.99 ± 0.00
	MiniCPM-V2-6B [73]	106.41 ± 4.72		15.08 ± 0.21	85.52 ± 0.34	14.46 ± 0.33	25.07 ± 0.51	10.61 ± 0.45
	Phi-4-MM-instruct [1]	52.78 ± 0.00		12.74 ± 0.00	87.72 ± 0.00	12.39 ± 0.00	19.47 ± 0.00	7.08 ± 0.00
	Qwen25VL-32B [4]	41.53 ± 0.06		20.37 ± 0.09	90.95 ± 0.06	16.85 ± 0.05	34.22 ± 0.51	17.36 ± 0.65

importance of each input, providing insights into the model’s decision-making process. This approach facilitates reasoning analysis without requiring external captioning models or vision-language models.

Due to the space limit, we provide model training settings in supplementary material.

5. Results and Analysis

5.1. Main results

Table 2 reports 23 representative models on the Year-Guessr test split (11,087 images), including CNN-based, Transformer-based, CLIP-based, Closed VLMs, and Open VLMs. Metrics include MAE, Interval Accuracy within $\pm 5/100$ years (IA_5 , IA_{100}), and popularity-stratified IA_5 ($< 10^2$, $> 10^5$) with *Gain* defined as the difference between high- and low-popularity bins.

Ordinal regression improves fine-grained prediction. Our YearCLIP reduces MAE to 39.52, outperforming ConvNeXt-B (44.42) and Swin-B (47.65). Compared to GeoCLIP, which does not use ordinal regression, YearCLIP decreases MAE by 13.5% (45.69 → 39.52) while maintain-

ing competitive IA_5 and IA_{100} .

CLIP priors. Zero-shot CLIP achieves MAE 78.23, better than some open-source VLMs like LLaVA-v16-13B (194.07) and MiniCPM-V2-6B (106.41). Fine-tuned CLIP variants (GeoCLIP, NumCLIP, YearCLIP) consistently improve MAE and IA over CNN and Transformer baselines, highlighting the benefits of pre-training and fine-tuning.

Closed-source VLMs dominate. Top performers are Gemini1.5-Pro (MAE 33.08), Gemini2.0-Flash (MAE 33.91), and Grok2 (MAE 35.28). The best open-source model, Gemma3-27B, scores MAE 36.48. Other open-source models like LLaVA-v16-13B and InternVL2-26B lag considerably.

5.2. Popularity analysis

Table 2 shows IA_5 across five popularity bins based on Wikipedia page views. *Gain* is the difference in IA_5 between high ($> 10^5$) and low popularity ($< 10^2$) buildings.

General trend across models. Across CNNs, Transformers, and CLIP-based methods, highly popular buildings often yield worse accuracy. For example, ConvNeXt-B

Table 3. Mean Absolute Error (MAE) over (a) different regions and (b) different periods.

Method	Model	(a) Regions (Continents, MAE, ↓)					(b) Period (MAE, ↓)						
		Africa	Americas	Asia	Australia	Europe	1000–1150	1150–1400	1400–1600	1600–1800	1800–1900	1900–1950	1950–2024
CNN	ResNet-50 [24]	102.13	34.97	71.48	36.51	92.37	634.98	423.93	233.93	88.45	35.89	34.33	37.42
	ConvNeXt-B [37]	85.07	29.13	56.02	29.04	81.02	538.27	348.31	200.69	82.37	31.00	29.36	29.59
Transformer	ViT-B/16 [15]	100.41	31.23	72.55	32.49	88.99	236.50	199.25	218.36	93.35	32.75	30.76	30.68
	Swin-B [36]	104.53	31.08	69.26	29.93	86.10	557.44	402.18	218.38	79.21	32.53	32.69	30.07
CLIP-based	CLIP (zero-shot) [30]	148.98	53.72	116.45	64.07	125.09	228.83	215.68	185.49	99.41	71.56	81.51	54.12
	GeoCLIP [61]	100.53	27.12	62.40	25.33	87.22	197.04	145.22	171.61	81.67	41.83	32.69	30.07
	NumCLIP [16]	85.42	24.72	54.97	25.97	75.40	495.76	293.58	191.47	78.29	27.95	23.09	27.87
	YearCLIP (ours)	85.85	26.10	53.20	24.90	71.31	483.31	282.46	185.55	78.75	27.69	22.84	27.45
Closed VLMs	GPT4o-mini [2]	98.50	30.50	51.73	28.62	71.83	402.97	238.45	198.05	101.32	35.92	22.52	20.92
	Gemini1.5-pro [19]	67.71	27.91	60.17	30.22	66.27	386.86	226.83	157.73	70.83	26.22	16.88	21.40
	Gemini2.0-flash [20]	62.73	23.53	39.31	20.91	57.80	273.82	175.35	142.04	71.39	30.22	18.45	20.43
	Claude3-haiku [3]	91.85	25.34	63.81	30.23	78.77	284.09	290.85	202.74	107.55	39.21	26.88	26.64
	Grok2 [70]	72.00	23.92	45.87	19.75	62.58	165.47	62.58	165.47	79.22	35.61	19.04	23.51
OpenVLM	CogVLM2-19B [25]	105.48	28.77	56.77	26.85	72.89	388.90	243.09	199.62	85.26	34.26	27.44	23.35
	Gemma3-27B [58]	89.52	24.38	48.36	21.07	63.35	349.20	231.03	166.36	75.11	29.89	19.78	22.68
	GLM-4v-9B [65]	82.00	27.16	49.96	23.47	65.21	190.07	163.48	141.96	75.48	30.92	24.55	22.63
	InternVL2-26B [10]	163.84	52.50	114.88	275.11	184.64	539.88	418.39	346.32	48.03	121.22	93.48	102.90
	InternVL3-38B [10]	69.69	26.15	77.35	33.80	94.90	380.35	251.13	188.98	110.02	53.76	47.46	51.63
	LLaVA15-13B [35]	88.52	35.67	50.00	40.00	95.00	508.39	374.03	143.05	88.25	16.69	26.26	22.85
	LLaVA-v16-13B [35]	368.85	42.07	232.46	255.60	95.00	558.97	370.10	145.15	100.20	16.96	177.63	121.94
	MiniCPM-V2-6B [73]	205.98	33.83	88.98	116.66	147.21	456.59	271.43	144.95	84.76	30.86	76.92	144.65
	Phi-4-MM-instruct [1]	81.68	30.16	60.61	35.56	73.40	499.13	231.37	199.49	57.16	37.86	32.84	33.68
	Qwen25VL-32B [4]	61.08	30.64	42.64	26.46	68.44	411.36	199.96	192.55	94.20	36.95	21.22	21.76

(CNN) drops from 16.57% to 12.68% (Gain: -3.89%), Swin-B (Transformer) from 15.82% to 6.78% (-9.04%), and YearCLIP (CLIP-based) from 20.19% to 12.39% (-7.80%). This consistent decline suggests that iconic landmarks are harder to date, likely due to stylistic heterogeneity, renovations, or multiple historical narratives.

Popularity bias in VLMs. Both closed and open source VLMs display the opposite pattern, with consistently higher scores on popular buildings. Gemini2.0-Flash jumps from 24.23% to 58.41% (+34.18%), Gemini1.5-Pro from 26.76% to 43.36% (+16.60%), Grok2 from 25.77% to 42.48% (+16.71%), and Qwen2.5VL-32B from 16.85% to 34.22% (+17.36%). However, such gain reflects a strong popularity bias. Models likely exploit memorized associations from pre-training data, rather than demonstrating genuine architectural reasoning. This undermines their reliability, as performance becomes inflated on well-documented landmarks while offering little insight into less-known or underrepresented buildings.

5.3. Regional and Period Analysis

Table 3 reports MAE across five continents and eight historical periods, highlighting geographic and temporal biases.

Geographic Biases. Nearly every methods exhibit clear regional disparities: Americas and Australia yield the lowest MAE, while Africa and Europe are highest, with Asia in between. For example, Gemini2.0-flash achieves MAE = 23.53 (Americas) vs. 62.73 (Africa) and 57.80 (Europe). Similar trends appear in NumCLIP (Asia: 58.97, Europe: 71.31), reflecting skewed pre-training data.

Americas Dominance and YearCLIP. GeoCLIP, NumCLIP, and YearCLIP (ours) reach their lowest MAE in Americas (27.12, 26.97, 26.10), aligned with the dataset’s Americas-heavy distribution (63.3%, Figure 3). YearCLIP reduces this bias, achieving more balanced results across regions.

Temporal Trends and Early-Period Challenges. Table 3(b) shows a clear temporal effect: models achieve markedly lower MAE in later periods (e.g., Gemini1.5-pro: 386.86 in 1000–1150 vs. 16.88 in 1900–1950). Performance degrades sharply for the earliest periods, where MAE often exceeds 300 across methods (e.g., Qwen25VL-32B: 411.36 vs. 21.22). This gap likely stems from data scarcity, preservation bias, and the greater stylistic heterogeneity of ancient architecture, whereas abundant examples of modern buildings provide richer training signals.

5.4. Effect of Density and Renovation

Table 4 shows MAE by population density and renovation status. Population density, collected via GPWv4.11 API, is categorized as Rural (< 300 people/km², 27.33%), Semi-urban (300–1500, 26.30%), and Urban (> 1500, 46.37%). Renovation status, derived from 11,087 Wikipedia descriptions via LLM, includes Never (13.65%), Renovated (52.99%), and Rebuilt (0.25%).

Population Density. Semi-urban regions yield the lowest MAE across most models (YearCLIP: 36.22, Gemini1.5-pro: 30.07), while rural and urban areas are harder, likely due to architectural variety or mixed-era skylines. For example, Gemma3-27B: Rural 40.49 vs. Urban 35.76.

Table 4. Mean Absolute Error (MAE) over different population density and renovation types.

Method	Model	Population Density (MAE, ↓)			Renovation (MAE, ↓)		
		< 300	300–1500	> 1500	Never	Renovated	Rebuilt
CNN	ConvNeXt-B [37]	47.15	40.63	44.32	33.11	46.50	68.46
Transformer	Swin-B [36]	51.17	43.59	47.24	37.09	50.30	70.82
CLIP-based	YearCLIP (ours)	42.67	36.22	39.04	30.62	41.84	59.04
Closed VLMs	Gemini1.5-pro [19]	37.11	30.07	32.07	20.66	34.99	57.36
OpenVLM	Gemma3-27B [58]	40.49	32.63	35.76	24.64	37.96	61.13

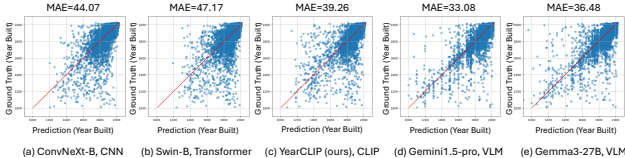


Figure 5. **Prediction error scatter plots for representative models.** (a) ConvNeXt-B (CNN), (b) Swin-B (Transformer), (c) YearCLIP (ours, CLIP-based), (d) Gemini1.5-pro (VLM), and (e) Gemma3-27B (VLM). The horizontal axis shows predicted construction year, vertical axis shows groundtruth. Each point represents a single building. The red diagonal line indicates perfect prediction.

Renovation Status. MAE is lowest for never-renovated buildings (Gemini1.5-pro: 20.66), increases for renovated ones (34.99), and peaks for rebuilt cases (57.36). Reconstructions may erase original architectural cues, making year prediction unreliable.

5.5. Prediction distribution

Figure 5 compares the prediction errors of five models, including ConvNeXt-B, Swin-B, YearCLIP, Gemini1.5-pro, and Gemma3-27B. CNN (ConvNeXt-B) and Transformer (Swin-B) show larger deviations, especially for pre-1600 buildings. YearCLIP yields predictions closer to the diagonal, indicating higher accuracy across periods. VLMs (Gemini1.5-pro, Gemma3-27B) cluster tightly along the diagonal, benefiting from linguistic and geographic context, though accuracy remains higher for post-1800 buildings due to temporal imbalance in training data.

5.6. Explainability

Figure 6 shows the output of YearCLIP, a Reason-enhanced NumCLIP with additional location conditions. The explainable age prediction can reduce the MAE and provide a human-verifiable rationale for each prediction. The reasoning system identifies architectural features such as roof types, materials, and structural elements that most strongly influence the predicted construction year, offering transparency into the model’s decision-making process in comparison to NumCLIP.

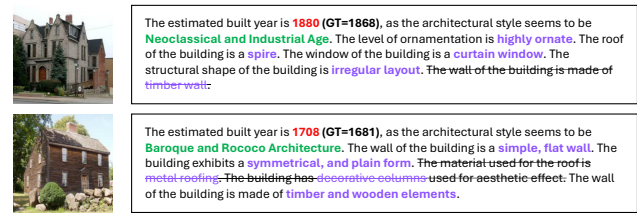


Figure 6. **Explainable age predictions with YEARCLIP.** Powered by Reason-enhanced NumCLIP, the system predicts **construction year** within ± 15 yr of **ground truth** and provides rationales that highlight **stylistic** and **historic** cues. CLIP baselines miss or misassign these signals, whereas our location + reason pipeline yields transparent, verifiable explanations.

6. Conclusion

We presented YEARGUESSR, the first CC BY-SA 4.0, large-scale dataset and benchmark for building-age estimation, plus an ordinal protocol, a popularity-aware metric, and a 30+ model study that reveals landmark-memorization bias while showing our NumCLIP-Loc system halves MAE over decade classification. The resource can aid heritage preservation, retrofit planning, and disaster inspection, yet it might also help locate vulnerable sites or reinforce regional bias. Safeguards include removal of non-free images, an accompanying responsible-use data card, and public bias metrics; closed-source VLMs are accessed via documented prompts without redistributing weights.

Limitations and Future Work. The dataset is geographically and temporally skewed toward modern examples, limiting generalization to underrepresented regions and early styles. Labels are also based on original construction years, even for substantially renovated or rebuilt buildings, introducing noise. We aim to address these issues by expanding non-Western and early-period coverage (e.g., integrating CMAB [79], targeted collection for low-resource regions), digitizing pre-1600 records, and adding explicit renovation/temporal-segmentation labels. To mitigate data scarcity, we plan to fine-tune diffusion priors for synthetic augmentation [59], and explore active learning, debiasing, and expert validation to improve robustness and reproducibility.

Acknowledgements. This research was funded by the National Science and Technology Council, Taiwan, under Grants NSTC 112-2222-E-A49-004-MY2 and 113-2628-E-A49-023-. The authors are grateful to Google, NVIDIA, and MediaTek Inc. for their generous donations. Yu-Lun Liu acknowledges the Yushan Young Fellow Program by the MOE in Taiwan.

References

- [1] Abdelrahman Abouelenin, Young Jin Kim, et al. Phi-4-mini technical report: Compact yet powerful multimodal language models via mixture-of-loras. *arXiv preprint arXiv:2503.01743*, 2025. 6, 7, 4, 5
- [2] Josh Achiam, Steven Adler, Sandhini Agarwal, Lama Ahmad, Ilge Akkaya, Florencia Leoni Aleman, Diogo Almeida, Janko Altenschmidt, Sam Altman, Shyamal Anadkat, et al. Gpt-4 technical report. *arXiv preprint arXiv:2303.08774*, 2023. 3, 6, 7, 4, 5
- [3] Anthropic Team. Claude 3 haiku: Our fastest model yet. <https://www.anthropic.com/news/clause-3-haiku>, 2024. 6, 7, 4, 5
- [4] Shuai Bai, Keqin Chen, Xuejing Liu, Jialin Wang, Wenbin Ge, Sibo Song, Kai Dang, Peng Wang, Shijie Wang, Jun Tang, Humen Zhong, Yuanzhi Zhu, Mingkun Yang, Zhaohai Li, Jianqiang Wan, Pengfei Wang, Wei Ding, Zheren Fu, Yiheng Xu, Jiabo Ye, Xi Zhang, Tianbao Xie, Zesen Cheng, Hang Zhang, Zhibo Yang, Haiyang Xu, and Junyang Lin. Qwen2.5-v1 technical report. *arXiv preprint arXiv:2502.13923*, 2025. 6, 7, 4, 5
- [5] Björn Barz and Joachim Denzler. Wikichurches: A fine-grained dataset of architectural styles with real-world challenges. *arXiv preprint arXiv:2108.06959*, 2021. 2
- [6] Favyen Bastani, Piper Wolters, Ritwik Gupta, Joe Ferdinando, and Aniruddha Kembhavi. Satlaspretrain: A large-scale dataset for remote sensing image understanding. In *Proceedings of the IEEE/CVF International Conference on Computer Vision*, pages 16772–16782, 2023. 2
- [7] Sean Bell, Paul Upchurch, Noah Snavely, and Kavita Bala. Material recognition in the wild with the materials in context database. In *Proceedings of the IEEE conference on computer vision and pattern recognition*, pages 3479–3487, 2015. 2
- [8] Filip Biljecki and Maximilian Sindram. Estimating building age with 3d gis. In *Proceedings of the 12th International 3D GeoInfo Conference 2017*, pages 17–24, 2017. 2
- [9] Wenzhi Cao, Vahid Mirjalili, and Sebastian Raschka. Rank consistent ordinal regression for neural networks with application to age estimation. *Pattern Recognition Letters*, 140: 325–331, 2020. 3, 4
- [10] Zhe Chen, Jiannan Wu, Wenhui Wang, Weijie Su, Guo Chen, Sen Xing, Muyan Zhong, Qinglong Zhang, Xizhou Zhu, Lewei Lu, et al. Internvl: Scaling up vision foundation models and aligning for generic visual-linguistic tasks. In *Proceedings of the IEEE/CVF Conference on Computer Vision and Pattern Recognition*, pages 24185–24198, 2024. 6, 7, 4, 5
- [11] Zhenfang Chen, Qinhong Zhou, Yikang Shen, Yining Hong, Zhiqing Sun, Dan Gutfreund, and Chuang Gan. Visual chain-of-thought prompting for knowledge-based visual reasoning. In *Proceedings of the AAAI Conference on Artificial Intelligence*, pages 1254–1262, 2024. 3
- [12] Brandon Clark, Alec Kerrigan, Parth Parag Kulkarni, Vicente Vivanco Cepeda, and Mubarak Shah. Where we are and what we’re looking at: Query based worldwide image geo-localization using hierarchies and scenes. In *Proceedings of the IEEE/CVF Conference on Computer Vision and Pattern Recognition*, pages 23182–23190, 2023. 2
- [13] Andrey Dimitrov and Mani Golparvar-Fard. Vision-based material recognition for automated monitoring of construction progress and generating building information modeling from unordered site image collections. *Advanced Engineering Informatics*, 28(1):37–49, 2014. 2
- [14] Nikolaos Dionelis, Nicolas Longépé, Alessandra Feliciotti, Mattia Marconcini, Devis Peressutti, Nika Oman Kadunc, Jaewan Park, Hagai Raja Sinulingga, Steve Andreas Immanuel, Ba Tran, et al. Building age estimation: A new multi-modal benchmark dataset and community challenge. *arXiv preprint arXiv:2502.13818*, 2025. 1, 2, 3
- [15] Alexey Dosovitskiy, Lucas Beyer, Alexander Kolesnikov, Dirk Weissenborn, Xiaohua Zhai, Thomas Unterthiner, Mohammad Dehghani, Matthias Minderer, Georg Heigold, Sylvain Gelly, et al. An image is worth 16x16 words: Transformers for image recognition at scale. *arXiv preprint arXiv:2010.11929*, 2020. 6, 7, 3
- [16] Yao Du, Qiang Zhai, Weihang Dai, and Xiaomeng Li. Teach clip to develop a number sense for ordinal regression. In *European Conference on Computer Vision*, pages 1–17. Springer, 2024. 2, 3, 5, 6, 7, 4
- [17] Marco Fiorucci, Marina Khoroshiltseva, Massimiliano Pontil, Arianna Traviglia, Alessio Del Bue, and Stuart James. Machine learning for cultural heritage: A survey. *Pattern Recognition Letters*, 133:102–108, 2020. 2
- [18] Huan Fu, Mingming Gong, Chaohui Wang, Kayhan Batmanghelich, and Dacheng Tao. Deep ordinal regression network for monocular depth estimation. In *Proceedings of the IEEE conference on computer vision and pattern recognition*, pages 2002–2011, 2018. 3
- [19] Gemini Team, Petko Georgiev, Ving Ian Lei, Ryan Burnell, Libin Bai, Anmol Gulati, Garrett Tanzer, Damien Vincent, Zhufeng Pan, Shibo Wang, Soroosh Mariooryad, Yifan Ding, Xinyang Geng, Fred Alcober, Roy Frostig, Mark Omernick, Lexi Walker, Cosmin Paduraru, Christina Sorokin, Andrea Tacchetti, Colin Gaffney, Samira Daruki, Olcan Serincoglu, Zach Gleicher, Juliette Love, Paul Voigtlaender, Rohan Jain, Gabriela Surita, Kareem Mohamed, Rory Blevins, Junwhan Ahn, Tao Zhu, Kornraphop Kawintiranon, Orhan Firat, Yiming Gu, Yujing Zhang, Matthew Rahtz, Manaal Faruqui, Natalie Clay, Justin Gilmer, JD Co-Reyes, Ivo Penchev, Rui Zhu, Nobuyuki Morioka, Kevin Hui, Krishna Haridasan, Victor Campos, Mahdis Mahdieh, Mandy Guo, Samer Hassan, Kevin Kilgour, Arpi Vezer, Heng-Tze Cheng, Raoul de Liedekerke, Siddharth Goyal, Paul Barham, DJ Strouse, Seb Noury, Jonas Adler, Mukund Sundararajan, Sharad Vikram, Dmitry Lepikhin, Michela Paganini, Xavier Garcia, Fan Yang, Dasha Valter, Maja Trebacz, Kiran Vodrahalli, Chulayuth Asawaroengchai, Roman Ring, Norbert Kalb, Livio Baldini Soares, Siddhartha Brahma, David Steiner,

- Tianhe Yu, Fabian Mentzer, Antoine He, Lucas Gonzalez, Bibo Xu, Raphael Lopez Kaufman, Laurent El Shafey, Junhyuk Oh, Tom Hennigan, George van den Driessche, Seth Odoom, Mario Lucic, Becca Roelofs, Sid Lall, Amit Marathe, Betty Chan, Santiago Ontanon, Luheng He, Denis Teplyashin, Jonathan Lai, Phil Crone, Bogdan Damoc, Lewis Ho, Sebastian Riedel, Karel Lenc, Chih-Kuan Yeh, Aakanksha Chowdhery, Yang Xu, Mehran Kazemi, Ehsan Amid, Anastasia Petrushkina, Kevin Swersky, Ali Khodaei, Gowoon Chen, Chris Larkin, Mario Pinto, Geng Yan, Adria Puigdomenech Badia, Piyush Patil, Steven Hansen, Dave Orr, and M. Gemini 1.5: Unlocking multimodal understanding across millions of tokens of context. *arXiv preprint arXiv:2403.05530*, 2024. [6](#), [7](#), [8](#), [4](#), [5](#)
- [20] Gemini Team et al. Gemini 2.0: Advances in multimodal reasoning and robotics. *arXiv preprint arXiv:2503.20020*, 2025. [6](#), [7](#), [1](#), [3](#), [4](#), [5](#)
- [21] Tianchu Guo, Hui Zhang, ByungIn Yoo, Yongchao Liu, Youngjun Kwak, and Jae-Joon Han. Order regularization on ordinal loss for head pose, age and gaze estimation. In *Proceedings of the AAAI conference on artificial intelligence*, pages 1496–1504, 2021. [3](#)
- [22] Lukas Haas, Michal Skreta, Silas Alberti, and Chelsea Finn. Pigeon: Predicting image geolocations. In *Proceedings of the IEEE/CVF Conference on Computer Vision and Pattern Recognition*, pages 12893–12902, 2024. [3](#)
- [23] James Hays and Alexei A Efros. Im2gps: estimating geographic information from a single image. In *2008 ieee conference on computer vision and pattern recognition*, pages 1–8. IEEE, 2008. [2](#)
- [24] Kaiming He, Xiangyu Zhang, Shaoqing Ren, and Jian Sun. Deep residual learning for image recognition. *Proceedings of the IEEE conference on computer vision and pattern recognition*, pages 770–778, 2016. [6](#), [7](#), [3](#)
- [25] Wenyi Hong, Weihan Wang, Ming Ding, Wenmeng Yu, Qingsong Lv, Yan Wang, Yean Cheng, Shiyu Huang, Junhui Ji, Zhao Xue, et al. Cogvlm2: Visual language models for image and video understanding, 2024. [6](#), [7](#), [4](#), [5](#)
- [26] Peng-Hao Hsu, Ke Zhang, Fu-En Wang, Tao Tu, Ming-Feng Li, Yu-Lun Liu, Albert YC Chen, Min Sun, and Cheng-Hao Kuo. Openm3d: Open vocabulary multi-view indoor 3d object detection without human annotations. In *Proceedings of the IEEE/CVF International Conference on Computer Vision*, pages 8688–8698, 2025. [3](#)
- [27] Chih Yao Hu, Yang-Sen Lin, Yuna Lee, Chih-Hai Su, Jie-Ying Lee, Shr-Ruei Tsai, Chin-Yang Lin, Kuan-Wen Chen, Tsung-Wei Ke, and Yu-Lun Liu. See, point, fly: A learning-free vlm framework for universal unmanned aerial navigation. In *Conference on Robot Learning*, pages 4697–4708. PMLR, 2025. [3](#)
- [28] Jie-Ying Lee, Yi-Ruei Liu, Shr-Ruei Tsai, Wei-Cheng Chang, Chung-Ho Wu, Jiewen Chan, Zhenjun Zhao, Chieh Hubert Lin, and Yu-Lun Liu. Skyfall-gs: Synthesizing immersive 3d urban scenes from satellite imagery. *arXiv preprint arXiv:2510.15869*, 2025. [2](#)
- [29] Ling Li, Yu Ye, Bingchuan Jiang, and Wei Zeng. Georeasoner: Geo-localization with reasoning in street views using a large vision-language model. In *Forty-first International Conference on Machine Learning*, 2024. [3](#), [5](#)
- [30] Wanhu Li, Xiaoke Huang, Jiwen Lu, Jianjiang Feng, and Jie Zhou. Learning probabilistic ordinal embeddings for uncertainty-aware regression. In *Proceedings of the IEEE/CVF conference on computer vision and pattern recognition*, pages 13896–13905, 2021. [3](#), [7](#)
- [31] Wanhu Li, Xiaoke Huang, Zheng Zhu, Yansong Tang, Xiu Li, Jie Zhou, and Jiwen Lu. Ordinalclip: Learning rank prompts for language-guided ordinal regression. *Advances in Neural Information Processing Systems*, 35:35313–35325, 2022. [3](#)
- [32] Yan Li, Yiqun Chen, Abbas Rajabifard, Kourosh Khoshelham, and Mitko Aleksandrov. Estimating building age from google street view images using deep learning (short paper). In *10th international conference on geographic information science (GIScience 2018)*, pages 40–1. Schloss Dagstuhl–Leibniz-Zentrum für Informatik, 2018. [2](#)
- [33] Dingkang Liang, Jiahao Xie, Zhikang Zou, Xiaoqing Ye, Wei Xu, and Xiang Bai. Crowdclip: Unsupervised crowd counting via vision-language model. In *Proceedings of the IEEE/CVF conference on computer vision and pattern recognition*, pages 2893–2903, 2023. [3](#)
- [34] Hantang Liu, Yinghao Xu, Jialiang Zhang, Jianke Zhu, Yang Li, and Steven CH Hoi. Deepfacade: A deep learning approach to facade parsing with symmetric loss. *IEEE Transactions on Multimedia*, 22(12):3153–3165, 2020. [2](#)
- [35] Haotian Liu, Chunyuan Li, Yuheng Li, and Yong Jae Lee. Improved baselines with visual instruction tuning, 2023. [6](#), [7](#), [4](#), [5](#)
- [36] Ze Liu, Yutong Lin, Yue Cao, Han Hu, Yixuan Wei, Zheng Zhang, Stephen Lin, and Baining Guo. Swin transformer: Hierarchical vision transformer using shifted windows. *Proceedings of the IEEE/CVF international conference on computer vision*, pages 10012–10022, 2021. [6](#), [7](#), [8](#), [3](#)
- [37] Zhuang Liu, Hanzi Mao, Chao-Yuan Wu, Christoph Feichtenhofer, Trevor Darrell, and Saining Xie. A convnet for the 2020s. *Proceedings of the IEEE/CVF Conference on Computer Vision and Pattern Recognition*, pages 11976–11986, 2022. [6](#), [7](#), [8](#), [3](#)
- [38] Jose Llamas, Pedro M. Lerones, Roberto Medina, Eduardo Zalama, and Jaime Gómez-García-Bermejo. Classification of architectural heritage images using deep learning techniques. *Applied Sciences*, 7(10):992, 2017. [2](#)
- [39] Grace Luo, Giscard Biamby, Trevor Darrell, Daniel Fried, and Anna Rohrbach. G* 3: Geolocation via guidebook grounding. *arXiv preprint arXiv:2211.15521*, 2022. [2](#)
- [40] Andjelo Martinović, Markus Mathias, Julien Weissenberg, and Luc Van Gool. A three-layered approach to facade parsing. In *European conference on computer vision*, pages 416–429. Springer, 2012. [2](#)
- [41] Markus Mathias, Andjelo Martinovic, Julien Weissenberg, Simon Haegler, and Luc Van Gool. Automatic architectural style recognition. *The International Archives of the Photogrammetry, Remote Sensing and Spatial Information Sciences*, 38:171–176, 2012.

- [42] Markus Mathias, Andjelo Martinović, and Luc Van Gool. Atlas: A three-layered approach to facade parsing. *International Journal of Computer Vision*, 118(1):22–48, 2016. 2
- [43] Ben Mildenhall, Pratul P Srinivasan, Matthew Tancik, Jonathan T Barron, Ravi Ramamoorthi, and Ren Ng. Nerf: Representing scenes as neural radiance fields for view synthesis. *Communications of the ACM*, 65(1):99–106, 2021. 3
- [44] Eric Muller-Budack, Kader Pustu-Iren, and Ralph Ewerth. Geolocation estimation of photos using a hierarchical model and scene classification. In *Proceedings of the European conference on computer vision (ECCV)*, pages 563–579, 2018. 2
- [45] Florian Nachtigall, Nikola Milojevic-Dupont, Felix Wagner, and Felix Creutzig. Predicting building age from urban form at large scale. *Computers, Environment and Urban Systems*, 105:102010, 2023. 2
- [46] Zhenxing Niu, Mo Zhou, Le Wang, Xinbo Gao, and Gang Hua. Ordinal regression with multiple output cnn for age estimation. In *Proceedings of the IEEE conference on computer vision and pattern recognition*, pages 4920–4928, 2016. 3, 4
- [47] Shraman Pramanick, Ewa M Nowara, Joshua Gleason, Carlos D Castillo, and Rama Chellappa. Where in the world is this image? transformer-based geo-localization in the wild. In *European Conference on Computer Vision*, pages 196–215. Springer, 2022. 2
- [48] Alec Radford, Jong Wook Kim, Chris Hallacy, Aditya Ramesh, Gabriel Goh, Sandhini Agarwal, Girish Sastry, Amanda Askell, Pamela Mishkin, Jack Clark, et al. Learning transferable visual models from natural language supervision. In *International conference on machine learning*, pages 8748–8763. PMLR, 2021. 3, 5, 6, 4
- [49] Julian F Rosser, Doreen S Boyd, Gavin Long, Sameh Zakhary, Yong Mao, and Darren Robinson. Predicting residential building age from map data. *Computers, Environment and Urban Systems*, 73:56–67, 2019. 2
- [50] Rasmus Rothe, Radu Timofte, and Luc Van Gool. Dex: Deep expectation of apparent age from a single image. In *Proceedings of the IEEE international conference on computer vision workshops*, pages 10–15, 2015. 3
- [51] Paul-Edouard Sarlin, Eduard Trulls, Marc Pollefeys, Jan Hosang, and Simon Lynen. Snap: Self-supervised neural maps for visual positioning and semantic understanding. *Advances in Neural Information Processing Systems*, 36:7697–7729, 2023. 3
- [52] Paul Hongseok Seo, Tobias Weyand, Jack Sim, and Bohyung Han. Cplanet: Enhancing image geolocation by combinatorial partitioning of maps. In *Proceedings of the European Conference on Computer Vision (ECCV)*, pages 536–551, 2018. 2
- [53] Saleh Seyedzadeh, Farzad Pour Rahimian, Ivan Glesk, and Marc Roper. Machine learning for estimation of building energy consumption and performance: a review. *Visualization in Engineering*, 6(1):5, 2018. 2
- [54] Shreya Shankar, Yoni Halpern, Eric Breck, James Atwood, Jimbo Wilson, and D Sculley. No classification without representation: Assessing geodiversity issues in open data sets for the developing world. *arXiv preprint arXiv:1711.08536*, 2017. 3
- [55] Nyeong-Ho Shin, Seon-Ho Lee, and Chang-Su Kim. Moving window regression: A novel approach to ordinal regression. In *Proceedings of the IEEE/CVF conference on computer vision and pattern recognition*, pages 18760–18769, 2022. 3
- [56] Krishna Srinivasan, Karthik Raman, Jiecao Chen, Michael Bendersky, and Marc Najork. Wit: Wikipedia-based image text dataset for multimodal multilingual machine learning. In *Proceedings of the 44th international ACM SIGIR conference on research and development in information retrieval*, pages 2443–2449, 2021. 2
- [57] Maoran Sun, Fan Zhang, and Fábio Duarte. Automatic building age prediction from street view images. In *2021 7th IEEE International Conference on Network Intelligence and Digital Content (IC-NIDC)*, pages 102–106. IEEE, 2021. 2
- [58] Gemma Team. Gemma 3. 2025. 6, 7, 8, 4, 5
- [59] Brandon Trabucco, Kyle Doherty, Max Gurin, and Ruslan Salakhutdinov. Effective data augmentation with diffusion models, 2023. 8
- [60] Johannes H Uhl and Stefan Leyk. Mtbf-33: A multi-temporal building footprint dataset for 33 counties in the united states (1900–2015). *Data in Brief*, 43:108369, 2022. 2
- [61] Vicente Vivanco Cepeda, Gaurav Kumar Nayak, and Mubarak Shah. Geoclip: Clip-inspired alignment between locations and images for effective worldwide geo-localization. *Advances in Neural Information Processing Systems*, 36:8690–8701, 2023. 3, 5, 6, 7, 4
- [62] Nam Vo, Nathan Jacobs, and James Hays. Revisiting im2gps in the deep learning era. In *Proceedings of the IEEE international conference on computer vision*, pages 2621–2630, 2017. 2
- [63] Angelina Wang, Alexander Liu, Ryan Zhang, Anat Kleiman, Leslie Kim, Dora Zhao, Iroha Shirai, Arvind Narayanan, and Olga Russakovsky. Revise: A tool for measuring and mitigating bias in visual datasets. *International Journal of Computer Vision*, 130(7):1790–1810, 2022. 3
- [64] Ning-Hsu Albert Wang and Yu-Lun Liu. Depth anywhere: Enhancing 360 monocular depth estimation via perspective distillation and unlabeled data augmentation. *Advances in Neural Information Processing Systems*, 37:127739–127764, 2024. 3
- [65] Weihan Wang, Qingsong Lv, Wenmeng Yu, Wenyi Hong, Ji Qi, Yan Wang, Junhui Ji, Zhuoyi Yang, Lei Zhao, Xixuan Song, Jiazheng Xu, Bin Xu, Juanzi Li, Yuxiao Dong, Ming Ding, and Jie Tang. Cogylm: Visual expert for pretrained language models, 2023. 6, 7, 4, 5
- [66] Zeyu Wang, Klint Qinami, Ioannis Christos Karakozis, Kyle Genova, Prem Nair, Kenji Hata, and Olga Russakovsky. Towards fairness in visual recognition: Effective strategies for bias mitigation. In *Proceedings of the IEEE/CVF conference on computer vision and pattern recognition*, pages 8919–8928, 2020. 3
- [67] Zhiqiang Wang, Dejia Xu, Rana Muhammad Shahroz Khan, Yanbin Lin, Zhiwen Fan, and Xingquan Zhu. Llmgeo: Benchmarking large language models on image geolocation in-the-wild. *arXiv preprint arXiv:2405.20363*, 2024. 3

- [68] Tobias Weyand, Ilya Kostrikov, and James Philbin. Planet-photo geolocation with convolutional neural networks. In *Computer Vision–ECCV 2016: 14th European Conference, Amsterdam, The Netherlands, October 11–14, 2016, Proceedings, Part VIII 14*, pages 37–55. Springer, 2016. 2
- [69] Ji-Jia Wu, Andy Chia-Hao Chang, Chieh-Yu Chuang, Chun-Pei Chen, Yu-Lun Liu, Min-Hung Chen, Hou-Ning Hu, Yung-Yu Chuang, and Yen-Yu Lin. Image-text co-decomposition for text-supervised semantic segmentation. In *Proceedings of the IEEE/CVF Conference on Computer Vision and Pattern Recognition*, pages 26794–26803, 2024. 2
- [70] xAI Team. Grok-2 beta release. <https://x.ai/blog/grok-2-beta-release>, 2024. 6, 7, 4, 5
- [71] Shixiong Xu, Chenghao Zhang, Lubin Fan, Gaofeng Meng, Shiming Xiang, and Jieping Ye. Addressclip: Empowering vision-language models for city-wide image address localization. In *European Conference on Computer Vision*, pages 76–92. Springer, 2024. 3
- [72] Hongji Yang, Xiufan Lu, and Yingying Zhu. Cross-view geo-localization with layer-to-layer transformer. *Advances in Neural Information Processing Systems*, 34:29009–29020, 2021. 3
- [73] Yuan Yao, Tianyu Yu, Ao Zhang, Chongyi Wang, Junbo Cui, Hongji Zhu, Tianchi Cai, Haoyu Li, Weilin Zhao, Zhihui He, et al. Minicpm-v: A gpt-4v level mllm on your phone. *arXiv preprint arXiv:2408.01800*, 2024. 6, 7, 4, 5
- [74] Zichao Zeng, June Moh Goo, Xinglei Wang, Bin Chi, Meihui Wang, and Jan Boehm. Zero-shot building age classification from facade image using gpt-4. *arXiv preprint arXiv:2404.09921*, 2024. 2
- [75] Matthias Zeppelzauer, Miroslav Despotovic, Muntaha Sakeena, David Koch, and Mario Döller. Automatic prediction of building age from photographs. In *Proceedings of the 2018 ACM on International Conference on Multimedia Retrieval*, pages 126–134, 2018. 2
- [76] Gaowei Zhang, Yue Pan, and Limao Zhang. Deep learning for detecting building façade elements from images considering prior knowledge. *Automation in Construction*, 133:104016, 2022. 2
- [77] Gengyuan Zhang, Yurui Zhang, Kerui Zhang, and Volker Tresp. Can vision-language models be a good guesser? exploring vlms for times and location reasoning. In *Proceedings of the IEEE/CVF Winter Conference on Applications of Computer Vision*, pages 636–645, 2024. 3
- [78] Renrui Zhang, Ziyao Zeng, Ziyu Guo, and Yafeng Li. Can language understand depth? In *Proceedings of the 30th ACM International Conference on Multimedia*, pages 6868–6874, 2022. 3
- [79] Yecheng Zhang, Huimin Zhao, and Ying Long. Cmab: A first national-scale multi-attribute building dataset in china derived from open source data and geoai. *arXiv preprint arXiv:2408.05891*, 2024. 2, 8
- [80] Wentian Zhao, Xinxiao Wu, and Xiaoxun Zhang. Memcap: Memorizing style knowledge for image captioning. In *Proceedings of the AAAI Conference on Artificial Intelligence*, pages 12984–12992, 2020. 3
- [81] Chenhao Zheng, Ayush Shrivastava, and Andrew Owens. Exif as language: Learning cross-modal associations between images and camera metadata. In *Proceedings of the IEEE/CVF Conference on Computer Vision and Pattern Recognition*, pages 6945–6956, 2023. 3
- [82] Sijie Zhu, Mubarak Shah, and Chen Chen. Transgeo: Transformer is all you need for cross-view image geo-localization. In *Proceedings of the IEEE/CVF Conference on Computer Vision and Pattern Recognition*, pages 1162–1171, 2022. 2

Beyond Memorization: A Multi-Modal Ordinal Regression Benchmark to Expose Popularity Bias in Vision-Language Models

Supplementary Material

7. Implementation details

Experimental setup. We split the dataset into training, validation, and test sets with 33,337, 11,122, and 11,087 samples, respectively, following a 6:2:2 ratio. All experiments are conducted on an NVIDIA RTX 4090 GPU. We use the following hyperparameters: learning rates for the image encoder and adapter are set to 1×10^{-5} , while the optimizer uses RAdam with a learning rate of 1×10^{-4} , and Adam betas of 0.9 and 0.999. The learning rate scheduler is multi-step with a step size of 60 and a gamma of 0.1. Loss weights are balanced with cross-entropy, KL divergence, and regression terms, each set to 1.0. We set the number of ranks to 7, use ViT-B/16 for both text and image encoders, and train with a batch size of 64 for 50 epochs at 16-bit precision.

Predefined Reasoning. In the experimental design, predefined prompts were generated with the assistance of the Gemini2.0 [20] model to facilitate the analysis of building age estimation. These prompts were crafted to produce textual rationales potentially relevant to architectural age judgment, subsequently categorized into distinct options. For instance, considering the building’s roof as a judgment criterion, Gemini2.0 [20] segmented the roof types into specific categories, including spire, dome, flat roof, sloped roof, gabled roof, mansard roof, and butterfly roof. An illustrative example is provided below table 5:

Table 5. Example roof types and their descriptions for building age estimation.

Roof Type	Description
spire	A sharply pointed roof emphasizing verticality and ornate detailing.
dome	A smoothly curved roof suggesting grandeur and centrality.
flat roof	A completely horizontal surface with an unobstructed and minimalist design.
sloped roof	A roof with a noticeable and functional inclination for water drainage and dynamic appearance.
gabled roof	A traditional peaked roof with a triangular profile that exudes symmetry.
mansard roof	A dual-pitched roof offering both elegance and additional living space.
butterfly roof	An inverted roof design that creates a V-shaped, modern, and unconventional look.

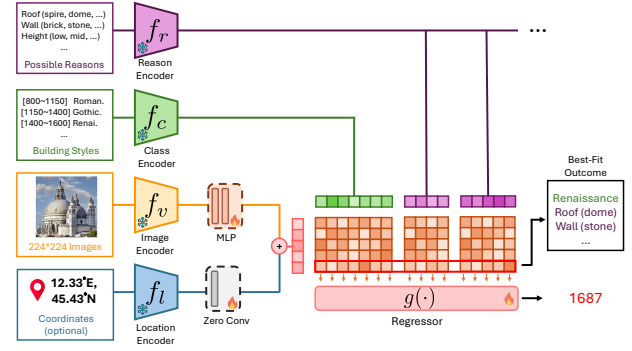


Figure 7. **YEARCLIP architecture.** An image encoder f_v (CLIP) extracts 224×224 facade features. We then fuse the feature with a GPS embedding from the location encoder f_l (RFF + MLP, optional input) via a learnable zero-convolution. Parallel text branches encode (i) seven coarse style classes f_c and (ii) a bank of reasoning prompts f_r describing roofs, walls, heights, etc. All frozen encoders feed a trainable regressor $g(\cdot)$ that performs coarse-to-fine ordinal regression. It outputs the predicted construction year (here 1687), selects the best-fit style/reason tokens, and outputs a readable rationale.

Beyond the roof, additional judgment criteria can be incorporated based on the task requirements, enabling further customization. Such enhancements enrich the input to the regressor, potentially improving the model’s performance and adaptability for architectural age estimation tasks.

8. Training Pipeline

This section outlines the training pipeline for the YearCLIP architecture, which predicts the construction year of buildings using a coarse-to-fine approach. The pipeline is divided into five parts, preceded by an introduction to define the inputs and pre-defined elements.

8.1. Introduction

The YearCLIP model in Figure 7 takes an image of a building and optional geographic coordinates as inputs. The image is a 224×224 pixel color image, while the coordinates are a pair of latitude and longitude values, which might not always be available. We also use pre-defined elements, including seven architectural styles (like Roman or Gothic), each linked to a specific historical period, and a set of reason prompts (like roof type or building material), where each prompt has subcategories (e.g., roof types include spire, dome, flat roof, etc.). The goal is to predict the building’s construction year and explain the reasoning behind the pre-

diction. The model uses several components: an image encoder, a location encoder, a class encoder for styles, a reason encoder for prompts, and a regressor to make the final prediction.

8.2. Input Processing

We process the input data in the following steps:

1. **Image Encoding:** The image encoder, based on CLIP, processes the building image to extract raw visual features:

$$\mathbf{z}_v^{\text{raw}} = f_v(I), \quad (1)$$

where I is the input image, and f_v is the image encoder. These raw features are then passed through a multi-layer perceptron (MLP) to obtain the final image embedding:

$$\mathbf{z}_v = \text{MLP}(\mathbf{z}_v^{\text{raw}}). \quad (2)$$

2. **Location Encoding:** If geographic coordinates are provided, the location encoder first transforms them into raw features via an MLP:

$$\mathbf{z}_l^{\text{raw}} = f_l(L), \quad (3)$$

where L is the pair of latitude and longitude values. These features are then processed by a learnable zero-convolution to produce the final location embedding:

$$\mathbf{z}_l = \text{ZeroConv}(\mathbf{z}_l^{\text{raw}}), \quad (4)$$

where ZeroConv ensures proper alignment for subsequent fusion.

3. **Combining Embeddings:** When coordinates are available, we combine the image embedding and location embedding by directly adding them:

$$\mathbf{z}_{\text{input}} = \mathbf{z}_v + \mathbf{z}_l, \quad (5)$$

where the addition is performed element-wise. If coordinates are missing, the input embedding is simply the image embedding \mathbf{z}_v . This allows the model to work even without location data.

8.3. Pre-Defined Elements

We define and process the pre-defined elements as follows:

1. **Building Styles Encoding:** We have seven architectural styles, each tied to a historical period: Roman (800–1150), Gothic (1150–1400), Renaissance (1400–1600), Baroque (1600–1750), Neoclassical (1750–1850), Modern (1850–1950), and Contemporary (1950–present). The class encoder processes each style to produce an embedding:

$$\mathbf{z}_{c_i} = f_c(s_i), \quad i = 1, 2, \dots, 7, \quad (6)$$

where s_i is a style (e.g., Roman), and f_c is the class encoder. This results in a set of embeddings for all seven styles.

2. **Reason Prompts Encoding:** We use reason prompts like roof type, material, and height, each with subcategories (e.g., roof types include spire, dome, flat roof, etc.; materials include stone, brick, etc.). The reason encoder processes each subcategory to create an embedding:

$$\mathbf{z}_{r_{jk}} = f_r(r_{jk}), \quad (7)$$

where r_{jk} is a subcategory (e.g., spire for roof type), and f_r is the reason encoder. This forms a collection of embeddings for all subcategories.

8.4. Coarse Stage

We measure how well the input matches the pre-defined elements by computing similarities:

1. **Style Similarity:** We calculate the similarity between the input embedding and each style embedding using cosine similarity:

$$\text{sim}_{c_i} = \text{sim}(\mathbf{z}_{\text{input}}, \mathbf{z}_{c_i}), \quad i = 1, 2, \dots, 7, \quad (8)$$

where sim measures the cosine similarity between two embeddings, resulting in a set of scores showing how well the input matches each style.

2. **Reason Similarity:** Similarly, we compute the similarity between the input embedding and each reason subcategory embedding:

$$\text{sim}_{r_{jk}} = \text{sim}(\mathbf{z}_{\text{input}}, \mathbf{z}_{r_{jk}}), \quad (9)$$

forming a set of scores for all subcategories.

8.5. Fine Regression

The regression process uses the similarity scores to predict the construction year:

1. **Preparing Input for Regressor:** We combine the style and reason similarity scores into a single vector for the regressor:

$$\mathbf{s} = [\text{sim}_{c_1}, \text{sim}_{c_2}, \dots, \text{sim}_{c_7}, \text{sim}_{r_{11}}, \text{sim}_{r_{12}}, \dots, \text{sim}_{r_{m_n}}], \quad (10)$$

where the vector includes all style similarities and all reason subcategory similarities.

2. **Computing Probabilities:** The regressor processes this vector to produce probabilities for each of the seven historical periods, indicating the likelihood that the building belongs to each period.

3. **Final Prediction:** The final predicted year is calculated as a weighted average of the midpoints of the historical periods, adjusted by the probabilities and a small confidence term:

$$\hat{y} = \sum_{i=1}^k p_i \cdot \frac{b_i}{1 + \delta_i}, \quad (11)$$

where p_i is the probability for the i -th period, b_i is the midpoint of that period, and δ_i is a small learnable parameter for stability.

8.6. Reasoning Importance

We analyze the importance of each reason to explain the prediction:

- Subcategory Importance:** We calculate an importance score for each reason subcategory by combining its similarity score with the regressor’s attention to the corresponding historical period.
- Selecting Key Subcategories:** For each reason (like roof or material), we pick the subcategory with the highest importance score. We also sum the importance scores of all subcategories for each reason to find the overall importance of that reason.
- Top Reasons:** We select the top five reasons with the highest overall importance, providing insights into the key factors (e.g., roof type: dome, material: stone) that influenced the predicted year.

8.7. Loss Function

To train the model, we use a combination of two loss terms:

- Fine-grained Cross-modal Ranking-based Contrastive Loss (FCRC):** Following NumCLIP [16], we adopt a ranking-based contrastive loss to enforce ordinal consistency between predicted and ground-truth labels. The FCRC loss is defined as:

$$\mathcal{L}_{\text{FCRC}}^z = - \sum_{i=1}^M \frac{1}{M} \log \left[\frac{f(z^i, w^i)}{f(z^i, w^i) + \sum_{j \neq i} \lambda_{i,j}^z f(z^i, w^j)} \right] \quad (12)$$

where $f(z^i, w^j) = \exp(\cos(z_i, w_j)/\tau)$ measures the similarity between image embedding z_i and text embedding w_j , and $\lambda_{i,j}^z$ denotes the regularisation weight of the j -th negative sample.

- Weighting of Negative Samples:** The weight parameter $\lambda_{i,j}$ is determined by the label distance between samples:

$$\lambda_{i,j} = \text{Norm}(\beta \cdot d_{i,j}), \quad d_{i,j} = |y_i - y_j|, \quad (13)$$

where y_i and y_j are the ground-truth labels of the anchor and negative samples, β is a scaling factor, and Norm ensures the weights sum to 1.

9. Full Table Results

9.1. Basic Method on Building Year Estimation

To evaluate the performance of different architectural models for building age estimation on the YearGuesser dataset [14], we conducted a comparative analysis based on the Mean Absolute Error (MAE) metric, as presented in Figure 8. This figure illustrates the MAE values achieved by a diverse set of models, categorized into three groups: CNN-based (green) [24, 37], Transformer-based (blue) [15, 36], and CLIP-based (yellow) methods. The MAE values, ranging from 40 to 60, are plotted along a horizontal axis, with each

model labeled at its corresponding MAE position. Notable CNN-based models include ResNet50 (MAE 54.59) [24], ResNet152 (MAE 47.70) [24], and ConvNeXt-L (MAE 42.34) [37], demonstrating a trend of improved accuracy with increased model complexity. Transformer-based models, such as ViT-B/16 (MAE 48.86) [15] and Swin-B (MAE 47.71) [36], show competitive performance, while CLIP-based models like GeoCLIP (MAE 44.32) [61] and NumCLIP (MAE 40.01) [16] exhibit the lowest MAE values, highlighting the efficacy of vision-language integration. This comparison underscores the trade-offs between model complexity, architectural design, and prediction accuracy, providing insights for selecting appropriate models for future tasks.

● CNN-based ● Transformer-based ● CLIP-based

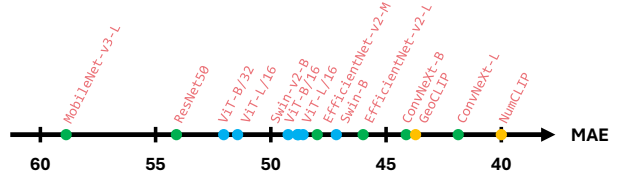


Figure 8. **Comparison of basic methods based on Mean Absolute Error (MAE).** The figure displays MAE values for various models, categorized by method type: CNN-based (green), Transformer-based (blue), and CLIP-based (yellow). Methods are positioned along the MAE axis, ranging from 40 to 60, with labels indicating model names.

9.2. Full Results of CLIP-based Model and VLMs

The following tables (6, 7, and 8) provide the complete experimental results corresponding to Results and Anaysis in the main paper. These tables extend the analysis by including a broader range of models, encompassing various model sizes and architectures. Specifically, Table 6 reports performance on basic metrics (Mean Absolute Error and Classification Accuracy) and interval accuracy across different year ranges. Table 7 details interval accuracy within ± 5 years across popularity intervals, while Table 8 presents the same metric across different continents. These comprehensive results offer deeper insights into the performance of models with varying capacities on the building age estimation task.

10. LLM Usage Statement

This work involved the use of Large Language Models (LLMs) in several limited capacities, none of which reached the level of contribution that would warrant co-authorship. The specific uses are detailed below:

Predefined Reasoning Prompt Generation (Section 4, Appendix 7): Gemini2.0 [20] was used to generate predefined reasoning prompts for architectural age estimation

Table 6. Performance on Basic metrics and Accuracy within intervals.

Method	Basic		Interval Accuracy (IA)			
	MAE (↓)	CLS Acc (↑)	≤ 5 yrs (↑)	≤ 20 yrs (↑)	≤ 50 yrs (↑)	≤ 100 yrs (↑)
CLIP (zero-shot) [48]	78.23	55.43	12.78	36.81	58.05	78.55
GeoCLIP [61]	44.32	70.16	24.48	56.25	77.80	89.57
NumCLIP [16]	40.01	69.12	19.35	54.40	79.53	91.76
YearCLIP (ours)	39.38	68.67	18.50	54.17	79.52	91.85
GPT4o-mini [2]	42.69	68.95	22.75	54.51	76.43	89.62
Gemini1.5-pro [19]	33.08	74.09	28.18	63.50	83.27	93.14
Gemini2.0-flash [20]	33.91	73.50	29.71	62.61	82.46	92.75
Claude3-haiku [3]	47.88	62.03	16.13	47.42	73.21	88.47
Grok2 [70]	35.28	73.74	27.57	61.31	81.90	93.02
CogVLM2-19B [25]	41.50	66.74	18.39	52.34	77.65	90.74
Gemma3-4B [58]	40.97	68.05	22.78	55.14	78.76	91.67
Gemma3-12B [58]	36.97	70.67	24.82	58.10	80.71	92.28
Gemma3-27B [58]	36.48	70.83	25.58	58.46	81.28	92.53
GLM-4v-9B [65]	38.27	70.85	20.03	55.60	79.79	91.73
InternVL2-2B [10]	145.68	48.75	9.73	31.92	58.97	79.28
InternVL2-4B [10]	67.15	55.46	12.00	37.76	66.91	85.88
InternVL2-8B [10]	196.69	52.94	11.62	36.36	62.08	78.44
InternVL2-26B [10]	77.22	63.49	16.84	47.79	73.38	87.71
InternVL3-2B [10]	101.10	52.98	10.98	35.39	64.72	83.70
InternVL3-8B [10]	54.24	60.24	16.20	46.26	73.39	89.60
InternVL3-9B [10]	58.95	60.71	15.60	45.60	72.50	88.36
InternVL3-14B [10]	63.35	59.61	16.61	46.32	72.10	88.22
InternVL3-38B [10]	61.79	68.47	20.37	53.06	77.40	90.19
LLaVA15-7B [35]	51.05	59.48	13.46	44.40	72.09	87.50
LLaVA15-13B [35]	60.08	61.52	10.72	36.26	66.76	84.24
LLaVA-v16-7B [35]	52.01	60.32	13.68	42.48	71.39	88.14
LLaVA-v16-13B [35]	169.21	58.06	12.34	39.83	65.82	81.69
MiniCPM-V2-6B [73]	107.01	60.02	15.09	45.03	69.99	85.75
Phi-4-MM-instruct [1]	52.78	55.32	12.74	42.10	70.86	87.72
Qwen25VL-3B [4]	91.38	63.57	16.54	49.42	74.46	88.63
Qwen25VL-7B [4]	40.06	70.21	19.88	53.86	77.42	91.10
Qwen25VL-32B [4]	41.66	67.02	20.31	52.97	77.05	90.91

analysis. Specifically, the model helped categorize building features into structured prompts, such as roof types (spire, dome, flat roof, sloped roof, gabled roof, mansard roof, butterfly roof) and their corresponding descriptions as shown in Table 5. The LLM assisted in creating comprehensive categorical descriptions for various architectural elements including materials, heights, and structural features that serve as input to our reasoning system.

Dataset Annotation Assistance (Section 3): An LLM was employed to analyze building descriptions from Wikipedia to extract renovation status information, as mentioned in the renovation scenario analysis (Figure 3(d)). The LLM helped distinguish between *renovated* buildings (where original construction year remains valid) and *rebuilt* buildings (where construction year is redefined) from textual descriptions in the dataset.

Writing and Code Assistance: LLMs were used as general-purpose writing assistance tools for improving clarity, grammar, and style throughout the manuscript. Additionally, LLMs provided coding assistance for data processing, experimentation scripts, and visualization code. However, all core algorithmic contributions, experimental design, analysis, and scientific insights were conceived and developed by the human authors.

Scope of Usage: The LLM usage was limited to auxiliary tasks and did not involve research ideation, hypothesis generation, experimental design, result interpretation, or the core technical contributions of the paper. All scientific claims,

Table 7. Interval Accuracy within ±5 years over different popularity intervals.

Method	Views (Popularity)				
	< 10 ² (↑)	10 ² –10 ³ (↑)	10 ³ –10 ⁴ (↑)	10 ⁴ –10 ⁵ (↑)	> 10 ⁵ (↑)
CLIP (zero-shot) [48]	13.52	12.38	13.86	11.49	7.96
GeoCLIP [61]	25.49	23.60	22.92	19.67	20.35
NumCLIP [16]	22.25	20.65	18.03	14.25	16.81
YearCLIP (ours)	20.42	19.65	17.11	16.02	9.73
GPT4o-mini [2]	19.01	21.25	23.82	27.96	48.67
Gemini1.5-pro [19]	26.76	27.26	28.54	32.04	43.36
Gemini2.0-flash [20]	24.23	26.85	31.90	40.33	58.41
Claude3-haiku [3]	18.45	15.27	16.24	17.35	32.74
Grok2 [70]	25.77	25.98	29.55	29.50	42.48
CogVLM2-19B [25]	16.20	17.98	19.48	18.12	23.89
Gemma3-4B [58]	20.56	22.39	23.76	22.87	25.66
Gemma3-12B [58]	25.07	23.99	25.53	26.08	33.63
Gemma3-27B [58]	24.37	24.12	26.86	28.95	41.59
GLM-4v-9B [65]	17.32	19.48	20.84	21.99	25.66
InternVL2-2B [10]	9.01	10.01	9.35	9.83	9.73
InternVL2-4B [10]	7.46	11.29	13.26	14.81	15.93
InternVL2-8B [10]	8.87	11.17	12.13	13.37	20.35
InternVL2-26B [10]	15.07	15.90	17.86	19.23	27.43
InternVL3-2B [10]	7.89	10.16	12.33	12.60	18.58
InternVL3-8B [10]	13.38	15.70	16.87	18.45	21.24
InternVL3-9B [10]	15.07	15.22	15.98	15.80	25.66
InternVL3-14B [10]	14.08	15.73	17.77	18.23	30.97
InternVL3-38B [10]	17.46	19.36	21.59	23.76	24.78
LLaVA15-7B [35]	11.69	13.24	13.95	13.92	17.70
LLaVA15-13B [35]	7.61	9.64	12.71	11.71	18.58
LLaVA-v16-7B [35]	11.97	13.35	14.36	14.36	17.70
LLaVA-v16-13B [35]	13.10	11.99	12.91	11.93	15.04
MiniCPM-V2-6B [73]	14.37	14.91	15.28	15.14	24.78
Phi-4-MM-instruct [1]	12.39	12.31	12.34	12.60	19.47
Qwen25VL-3B [4]	15.92	15.59	18.03	16.35	22.12
Qwen25VL-7B [4]	18.73	19.00	20.81	21.55	30.09
Qwen25VL-32B [4]	16.62	18.57	22.43	24.64	33.63

methodological innovations, and experimental conclusions remain solely the intellectual contribution of the human authors. The authors take full responsibility for all content, including any LLM-generated text that has been reviewed and validated.

Table 8. Interval Accuracy within ± 5 years over different regions.

Method	Regions (Continents)				
	Africa (\uparrow)	Americas (\uparrow)	Asia (\uparrow)	Australia (\uparrow)	Europe (\uparrow)
CLIP (zero-shot) [48]	12.30	13.29	20.60	12.46	10.44
GeoCLIP [61]	15.57	26.99	23.08	25.84	13.94
NumCLIP [16]	10.66	23.19	17.37	19.15	10.97
YearCLIP (ours)	13.11	22.04	20.10	16.41	10.40
GPT4o-mini [2]	20.49	24.47	31.76	20.36	17.67
Gemini1.5-pro [19]	25.41	30.54	30.77	31.61	22.04
Gemini2.0-flash [20]	25.41	30.67	38.46	32.52	26.04
Claude3-haiku [3]	11.48	17.72	19.11	17.63	11.90
Grok2 [70]	25.41	29.85	31.76	31.31	21.21
CogVLM2-19B [25]	15.57	20.40	23.57	13.37	13.74
Gemma3-4B [58]	17.21	24.75	25.06	27.36	17.34
Gemma3-12B [58]	19.67	26.85	31.27	30.40	18.81
Gemma3-27B [58]	26.23	27.41	32.75	31.91	19.61
GLM-4v-9B [65]	25.41	21.32	27.30	14.89	16.34
InternVL2-2B [10]	7.38	10.44	13.15	7.90	7.87
InternVL2-4B [10]	15.57	12.46	19.85	13.37	9.67
InternVL2-8B [10]	14.75	12.18	14.89	16.72	8.97
InternVL2-26B [10]	10.66	18.64	20.84	18.54	12.20
InternVL3-2B [10]	10.66	11.19	19.85	13.07	8.94
InternVL3-8B [10]	13.11	17.03	24.81	19.15	12.90
InternVL3-9B [10]	11.48	16.50	22.08	17.93	12.40
InternVL3-14B [10]	16.39	17.70	23.08	16.41	13.14
InternVL3-38B [10]	13.11	21.86	30.02	25.23	15.21
LLaVA15-7B [35]	18.85	14.09	19.85	15.20	10.77
LLaVA15-13B [35]	18.03	10.31	21.59	10.94	9.94
LLaVA-v16-7B [35]	13.93	15.19	16.63	15.81	9.60
LLaVA-v16-13B [35]	13.11	13.85	14.14	14.89	8.24
MiniCPM-V2-6B [73]	13.93	16.34	19.60	17.02	11.37
Phi-4-MM-instruct [1]	12.30	13.35	17.62	12.77	10.67
Qwen25VL-3B [4]	18.85	18.02	20.35	13.37	12.84
Qwen25VL-7B [4]	16.39	20.93	27.30	17.63	16.81
Qwen25VL-32B [4]	19.67	21.33	31.02	19.76	16.57

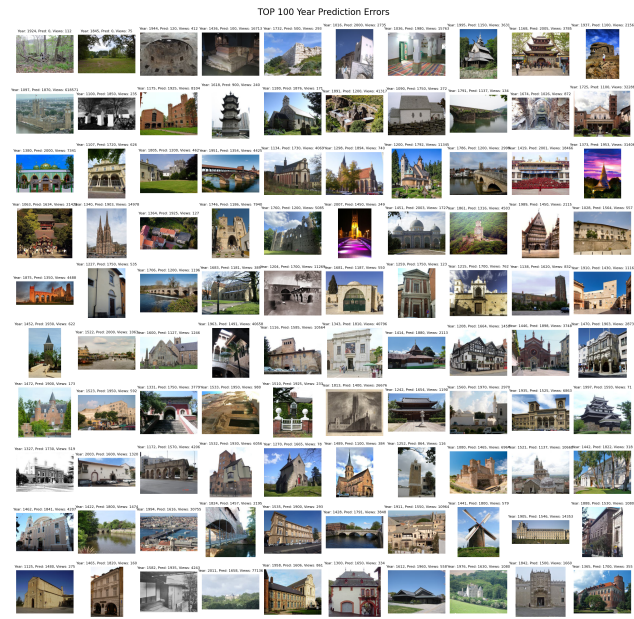


Figure 9. Top 100 prediction errors by Gemini2.0-Flash. This figure shows the 100 building images with the highest Mean Absolute Error (MAE) when predicted by Gemini2.0-Flash. Each image is labeled with the ground truth year (Year), predicted year (Pred), and Wikipedia page views (Views) as popularity indicator. These challenging cases illustrate common failure modes including ancient buildings, heavily renovated structures, and architecturally ambiguous facades.